Journal of Applied Physics

Competitive gettering of iron in silicon photovoltaics: Oxide precipitates versus phosphorus diffusion

Cite as: J. Appl. Phys. **116**, 053514 (2014); https://doi.org/10.1063/1.4892015
Submitted: 27 June 2014 . Accepted: 21 July 2014 . Published Online: 04 August 2014

J. D. Murphy, R. E. McGuire, K. Bothe, V. V. Voronkov, and R. J. Falster

ARTICLES YOU MAY BE INTERESTED IN

The effect of oxide precipitates on minority carrier lifetime in n-type silicon
Journal of Applied Physics **118**, 215706 (2015); https://doi.org/10.1063/1.4936852

The effect of oxide precipitates on minority carrier lifetime in p-type silicon
Journal of Applied Physics **110**, 053713 (2011); https://doi.org/10.1063/1.3632067

On the mechanism of recombination at oxide precipitates in silicon
Applied Physics Letters **102**, 042105 (2013); https://doi.org/10.1063/1.4789858

© 2014 Author(s).

AIP Publishing

Competitive gettering of iron in silicon photovoltaics: Oxide precipitates versus phosphorus diffusion

J. D. Murphy,[1,a)] R. E. McGuire,[2] K. Bothe,[3] V. V. Voronkov,[4] and R. J. Falster[4]
[1]School of Engineering, University of Warwick, Coventry CV4 7AL, United Kingdom
[2]Department of Materials, University of Oxford, Parks Road, Oxford OX1 3PH, United Kingdom
[3]Institut für Solarenergieforschung Hameln/Emmerthal, Am Ohrberg 1, 31860 Emmerthal, Germany
[4]SunEdison, viale Gherzi 31, 28100 Novara, Italy

(Received 27 June 2014; accepted 21 July 2014; published online 4 August 2014)

Experiments have been conducted to understand the behaviour of iron in silicon containing oxide precipitates and associated defects (dislocations and stacking faults), which is subjected to phosphorus diffusion gettering. Injection-dependent minority carrier lifetime measurements are analysed to provide quantitative information on the degree to which the precipitates and associated defects are decorated with iron impurities. These data are correlated with bulk iron measurements based on the photodissociation of FeB pairs. Iron in the vicinity of oxide precipitates in samples with relatively low levels of bulk iron contamination ($< 5 \times 10^{12}\,\mathrm{cm}^{-3}$) can be gettered to some extent. Higher levels of bulk iron contamination ($> 1.2 \times 10^{13}\,\mathrm{cm}^{-3}$) result in irreversible behaviour, suggesting iron precipitation in the vicinity of oxide precipitates. Bulk iron is preferentially gettered to the phosphorus diffused layer opposed to the oxide precipitates and associated defects.
© *2014 Author(s). All article content, except where otherwise noted, is licensed under a Creative Commons Attribution 3.0 Unported License*. [http://dx.doi.org/10.1063/1.4892015]

I. INTRODUCTION

Silicon wafers for photovoltaics may contain extended crystal defects. In multicrystalline silicon (mc-Si), these include dislocations, precipitates, and grain boundaries. In monocrystalline silicon precipitates of light elements (particularly oxygen) are known to form[1,2] in vacancy-rich regions, which arise from rapid growth conditions. Strain fields surrounding extended defects provide low energy sites for segregation of impurity atoms and the formation of precipitates. The presence of impurities at extended defects enhances their recombination activity,[3–5] which, in the context of a photovoltaic solar cell, will reduce the conversion efficiency.

Gettering is routinely used in solar cell processing to remove impurities. Gettering processes, such as phosphorus diffusion gettering (PDG) and aluminium gettering, are highly effective in silicon wafers free of extended defects.[6,7] They are however less effective at improving lifetime in the vicinity of decorated extended defects.[8–10] This suggests that the interaction between impurities and extended defects is either not fully overcome during gettering processes, or that the impurities re-segregate to the extended defects during cooling. Previous work has studied the effect of PDG on grain boundaries,[11,12] and findings are apparently contradictory with grain boundaries becoming more[12] or less[11] recombination active after gettering. More experimental work is needed to ascertain whether or not impurities can be gettered away from different types of extended defect.

The formation of oxide precipitates has been linked to a substantial efficiency reduction in solar cells made from single-crystal silicon.[1] Such precipitates also form in mc-Si wafers.[9,13] We have recently shown a strong correlation between the quantity of iron segregated to the oxide precipitates and associated defects (surrounding dislocations and stacking faults) and the resulting recombination activity.[5] As solar silicon is at risk of contamination by transition metal impurities from the crucible or during cell processing, it is important to understand how the interaction of impurities with oxide precipitates evolves during cell processing.

Linking the recombination activity of decorated extended defects to bulk material properties is not straightforward. In this paper, we present results using a methodology which relies on the analysis of injection-dependent minority carrier lifetime measurements[14] and our prior correlation between recombination activity and the amount of iron segregated to oxide precipitates and associated defects.[5] Combining this with well-established techniques for measuring bulk iron concentrations by photodissociation of iron boron pairs[15–17] enables the simultaneous quantification of levels of iron in the bulk and that segregated to oxide precipitates and associated defects. This allows for the study of the efficacy of PDG at removing iron from oxide precipitates and associated defects, and the bulk.

II. EXPERIMENTAL METHODS

A. Sample preparation

High purity single-crystal Czochralski silicon wafers with a boron concentration of 7 to $8 \times 10^{15}\,\mathrm{cm}^{-3}$ were subjected to an oxygen precipitation process, similar to that previously described in Ref. 18. The $\sim 700\,\mu\mathrm{m}$ thick wafers were cross-sectioned and then subjected to a defect revealing etch, which allowed the oxide precipitate density to be determined. Samples measuring 3.5 cm by 3.5 cm were cut from

[a)]john.d.murphy@warwick.ac.uk

 © Author(s) 2014

regions of material in which the oxide precipitate density was $\sim 1 \times 10^9\,cm^{-3}$. The defect revealing etch demonstrated that a region near both sample surfaces was denuded of oxide precipitates, and this ranged from 16 to 33 μm deep. The denuded zone was removed by a planar chemical etch comprising HNO_3 (70%), CH_3COOH (100%), and HF (40%) in the ratio 75:17:8.

B. Processing sequence and lifetime measurements

Each sample was subjected to a series of processing steps, as illustrated in Figure 1. The purpose of Stage 1 was to characterise the initial conditions in the sample after denuded zone removal. In Stage 2, the samples were intentionally contaminated with iron using methods described in Refs. 19 and 20. Samples with very similar defect contents (oxide precipitate density and initial bulk iron contamination level) were annealed at temperatures ranging from 625 to 900 °C to provide a set of samples with different levels of iron. Sufficient time was left for iron diffusion throughout the sample.[20] After annealing the samples were cooled rapidly (to below 100 °C in $\sim$10 s). The iron silicide layer, which had formed at the surface, was removed by etching in tetramethylammonium hydroxide (TMAH) for 40 min at $\sim$80 °C. In Stage 3, the samples are subjected to a PDG process, which is described in more detail in Ref. 21. The PDG temperature profile is plotted in Ref. 21 and includes a 850 °C step for 72 min, followed by a 875 °C step for 10 min. Some samples are subjected to Stage 4, which is a repeat of Stage 3.

At the end of each processing stage, samples were passivated with silicon nitride grown by direct plasma enhanced chemical vapour deposition (PECVD) at 350 °C in an Oxford Instruments Plasmalab 80 Plus at the University of Oxford. Lifetime was measured by quasi-steady-state photoconductance (QSS-PC) using a Sinton WCT-120 lifetime tester.[22] Two lifetime measurements were made: one immediately after dissociation of FeB pairs by multiple flashes of light; another sufficiently long enough afterwards for the FeB pairs to have re-formed. The lifetime change was analysed to give the bulk interstitial iron concentration in the samples, using a specific method described in Ref. 18. Before entering the next sample processing stage, the silicon nitride passivation film was removed with concentrated HF.

C. Analysis of injection-dependent minority carrier lifetime data

The measured minority carrier lifetime with the FeB pairs in a dissociated state, $\tau_{measured}$, was corrected for other known recombination mechanisms to a residual lifetime, $\tau_{residual}$, defined according to

$$\frac{1}{\tau_{residual}} = \frac{1}{\tau_{measured}} - \left(\frac{1}{\tau_{band-to-band}} + \frac{1}{\tau_{CE\ Auger}} + \frac{1}{\tau_{Fe_i}}\right), \quad (1)$$

where $\tau_{band\text{-}to\text{-}band}$ is the lifetime due to band-to-band (radiative) recombination, $\tau_{CE\ Auger}$ is the lifetime due to Coulomb-enhanced Auger recombination, and τ_{Fe_i} is the lifetime due to recombination at interstitial iron. Details of these corrections are given in Ref. 18.

Throughout this study, we use a linear formulation of Shockley-Read-Hall (SRH) statistics (described in detail in Ref. 14), where $\tau_{residual}$ is plotted as a function of $X = n/p$, where n is the total electron concentration and p is the total

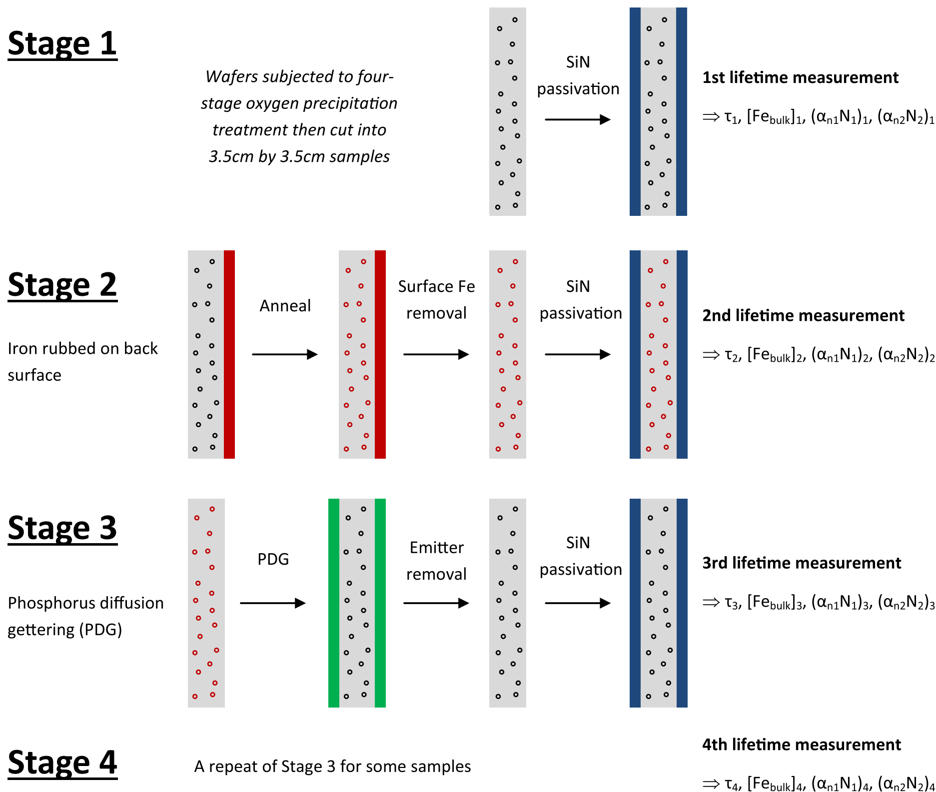

FIG. 1. Sequence of processing conditions.

hole concentration. Our previous work has shown that recombination at iron-contaminated oxide precipitates can be parameterised in terms of two independent SRH centres,[5,14,21] referred to as simply "Defect 1" and "Defect 2." If $\tau_{residual}$ is only determined by these two centres, it can be expressed as

$$\tau_{residual} = \left(\left(\frac{1}{N_1 \alpha_{n1}} \left[1 + \frac{Q_1 n_1}{p_0} + \frac{p_1}{p_0} + X \left(Q_1 - \frac{Q_1 n_1}{p_0} - \frac{p_1}{p_0} \right) \right] \right)^{-1} + \left(\frac{1}{N_2 \alpha_{n2}} \left[1 + \frac{Q_2 n_2}{p_0} + \frac{p_2}{p_0} + X \left(Q_2 - \frac{Q_2 n_2}{p_0} - \frac{p_2}{p_0} \right) \right] \right)^{-1} \right)^{-1}, \quad (2)$$

where $n_i = N_C \exp\left(-\frac{(E_C - E_i)}{kT}\right)$ and $p_i = N_V \exp\left(-\frac{(E_T - E_i)}{kT}\right)$, where N_C and N_V are the density of states in the conduction and valence bands, respectively, and E_i is the energy level of the defect (the subscripts i take the value 1 or 2). For oxide precipitates, we have previously determined that E_1 lies at $E_V + 0.22$ eV and $E_2 = E_C - 0.08$ eV, and that $Q_1 = 157$ and $1/Q_2 = 1200$ at room temperature.[14] Equation (2) can be used to fit experimental lifetime curves with the fitting parameters $N_1\alpha_{n1}$ and $N_2\alpha_{n2}$. Our previous work shows the $N_i\alpha_{ni}$ to be proportional to the amount of iron segregated to the oxide precipitates.[5] Under the assumption that the capture coefficient (α_{ni}) is invariant, this $N_i\alpha_{ni}$ term is proportional to the state density (N_i) and, thus, provides a measure of the quantity of iron segregated to the oxide precipitates and associated defects.[5] Thus, an increase in $N_i\alpha_{ni}$ corresponds to an increase of Fe in the vicinity of the oxide precipitates.

III. RESULTS

Figure 2 shows $\tau_{residual}$ versus $X = n/p$ at selected iron contamination temperatures. The three, or in some cases four, curves for each contamination temperature correspond to the lifetime measured at the end of the three, or in some cases four, processing stages shown in Figure 1. That is τ_1 represents the residual lifetime after Stage 1 (before contamination), τ_2 represents the residual lifetime after Stage 2 (after contamination), τ_3 represents residual lifetime after Stage 3 (after PDG), and τ_4 when plotted represents residual lifetime after Stage 4 (after second PDG). The bulk iron concentration as measured by photodissociation of FeB pairs is given in the legend. Note that for the 875 °C and 900 °C data, it was not possible to measure the bulk iron concentration after Stages 2 and 3 due to low lifetimes, so a value of 3×10^{13} cm^{-3} (based on the approximate solubility) is assumed for the residual lifetime calculations although the effect of varying this parameter is small.

Figure 3 shows the residual lifetime plots grouped by the processing stage. Figure 3(a) shows the lifetimes before iron contamination (end of Stage 1). Although the samples have nominally equivalent distributions of oxide precipitates, variation arises due to uncertainties in measuring precipitate densities and the degree to which the as-received samples are unintentionally contaminated by iron or other impurities not accounted for. Figure 3(b) shows the lifetimes after iron contamination (end of Stage 2). Samples contaminated at 625 °C to 726 °C exhibit approximately the same lifetime after iron contamination. Samples contaminated at higher temperature have substantially lower lifetimes, which decrease in order of increasing contamination temperature (iron concentration), which is consistent with our previous work.[5,21] Figure 3(c) shows the lifetimes in samples after PDG (end of Stage 3). In the samples contaminated at 625 °C to 773 °C, the lifetime is higher than it was both before and after iron contamination. At 798 °C, the lifetime is improved by the PDG process, with the initial lifetime being almost recovered but not improved upon. At higher temperatures, the initial lifetime is not recovered by the PDG process.

Figure 4 shows the bulk iron concentration measured in the samples at the different processing stages. The bulk iron concentration after the oxide precipitate formation process (Stage 1) had a similar value in all the samples, at ~1–2 × 10^{12} cm^{-3}. After Stage 2, the bulk iron concentration was dependent upon the iron contamination temperature. Higher contamination temperatures (>750 °C) resulted in an increase in bulk iron concentration. As the initial bulk iron concentration exceeded the solubility of iron at the lower temperatures used, the result of the "contamination" process was actually a reduction in iron concentration for anneals at 726 °C and below. The bulk iron concentration at the end of Stage 2 has a similar temperature dependence to the solubility value in oxide precipitate-free material.[19,20] At the very highest temperatures (> 800 °C), the bulk iron concentration exceeds the solubility slightly. At all lower temperatures, the bulk iron concentration is lower than the solubility in precipitate-free material, and we have previously attributed this to iron segregation to precipitates during cooling.[5]

Figure 4 also shows the bulk iron concentration after one PDG process (Stage 3) and, for some samples, after a second PDG process (Stage 4). For temperatures of 674 °C and above, the first PDG process lowers the bulk iron concentration. At the very lowest temperatures (625 °C and 659 °C), the bulk iron concentration increases slightly after PDG. This could be because iron is released from the vicinity of oxide precipitates during the PDG process, but the gettering time is insufficient for all the iron to diffuse to the phosphorus diffused layers at the surfaces. The second PDG process lowers the bulk iron concentration further, to a level of not below ~1 × 10^{11} cm^{-3}.

The lifetime data plotted in Figures 2 and 3 generally have the same form of injection-dependence and can be fitted

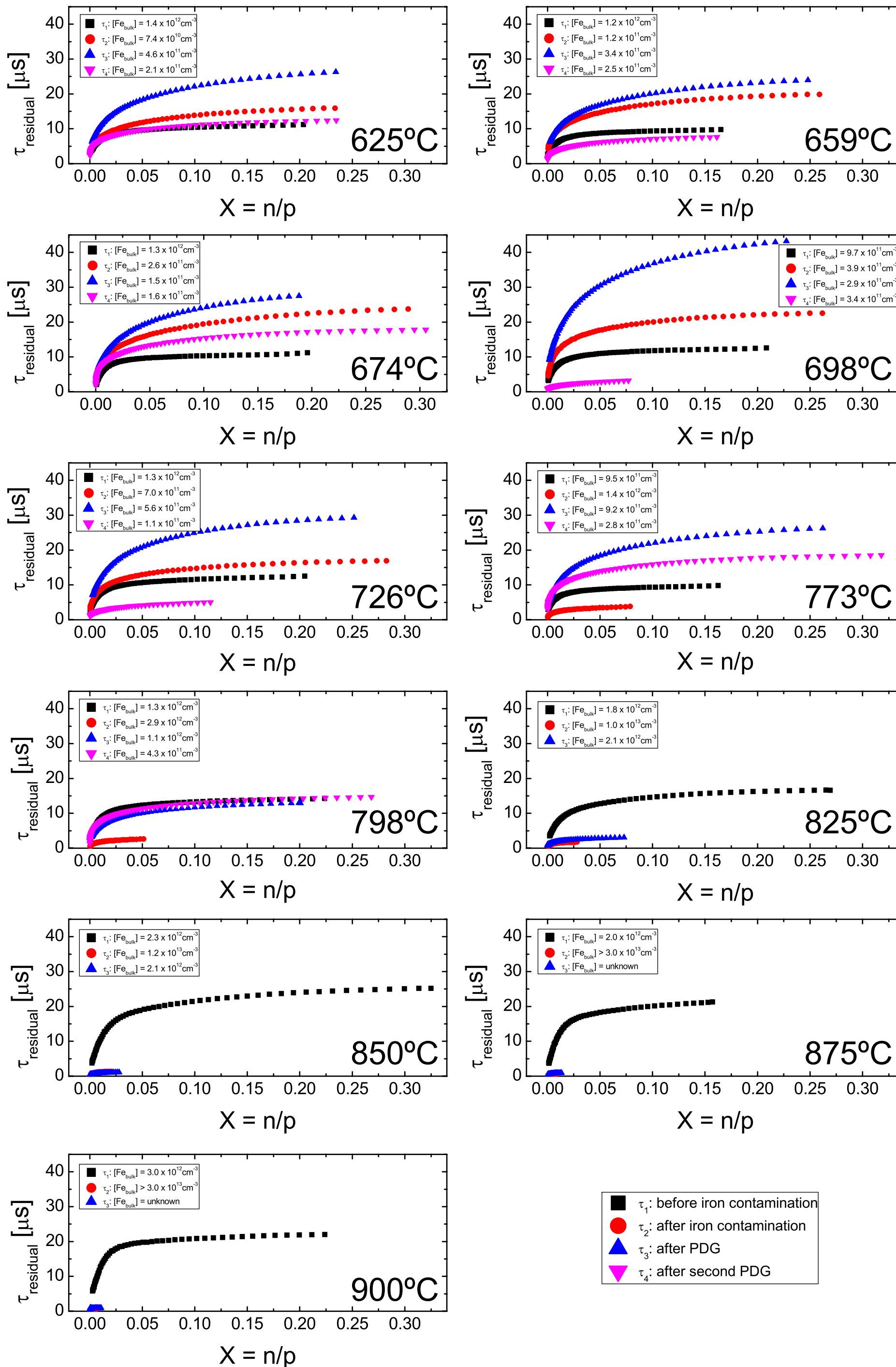

FIG. 2. Residual minority carrier lifetime, $\tau_{residual}$, versus $X = n/p$, where n and p are the total electron and hole concentrations, respectively. For each sample, lifetime curves are plotted: (i) after oxygen precipitation; (ii) after iron contamination at the temperature stated; and (iii) after PDG. Some samples were subjected to a second PDG process.

using Eq. (2) with our established parameters for recombination at iron-contaminated oxide precipitates. With the energy levels and cross-section ratios established previously,[14] the data can be fitted by varying the $N_1\alpha_{n1}$ and $N_2\alpha_{n2}$ terms, which have each been shown to be proportional to the quantity of iron segregated to the oxide precipitates and surrounding defects.[5] The $N_1\alpha_{n1}$ and $N_2\alpha_{n2}$ parameters required to fit the data after iron contamination and after the first PDG treatment are shown in Figure 5. It is not possible to determine these parameters for the samples contaminated at 875 °C and 900 °C as the lifetime data do not extend over a sufficient injection range, nor is it possible accurately to determine the bulk iron concentration.

For samples contaminated below ~800 °C, Figure 5 shows that the $N_1\alpha_{n1}$ and $N_2\alpha_{n2}$ parameters are reduced by the PDG process. This reduction is particularly pronounced in samples contaminated at 773 °C and 798 °C. For samples contaminated at 825 °C and 850 °C, the parameters do not decrease. In Sec. IV, these data are discussed in terms of iron segregation to the precipitates and associated defects.

IV. DISCUSSION

A. Iron decoration and minority carrier lifetime

The data presented in Figures 2 and 3 show that the residual lifetime in silicon containing iron-contaminated oxide

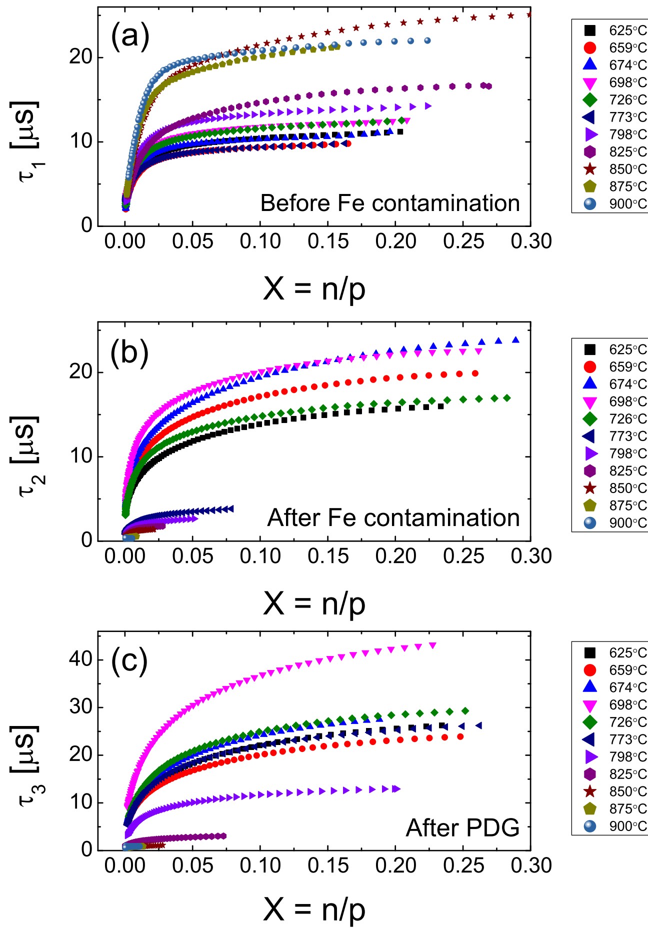

FIG. 3. Residual minority carrier lifetime versus $X = n/p$ at the end of: (a) Stage 1 (τ_1); (b) Stage 2 (τ_2); and (c) Stage 3 (τ_3). The legends give the iron contamination temperature.

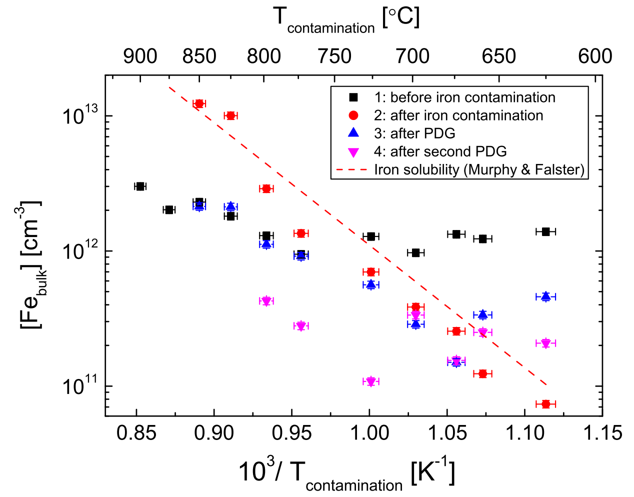

FIG. 4. The bulk iron concentration determined by photodissociation of iron boron pairs versus the temperature at which the sample was contaminated. The lifetimes were too low to enable accurate [Fe_{bulk}] measurements in the samples contaminated at 875 °C and 900 °C. The solubility of iron in oxide precipitate-free silicon is also plotted.[19,20] It is noted that this solubility line is only directly relevant to the Stage 2 data as the plot considers contamination (not PDG) temperature.

precipitates and associated defects can be increased by PDG in many cases. Figure 5 shows that the PDG process reduces the $N_1\alpha_{n1}$ and $N_2\alpha_{n2}$ parameters for samples contaminated with iron below ∼800 °C. These parameters correlate with iron segregated to oxide precipitates and associated defects;[5] thus, we conclude that iron becomes released from the oxide precipitates and associated defects during PDG of such samples. We have previously also shown this for a sample which has not been intentionally contaminated with iron.[21]

For low levels of iron (contamination <800 °C; solubility <5 × 10^{12} cm^{-3} (Refs. 19 and 20)) decoration of the oxide precipitates and associated defects appears to be a reversible process. Iron decoration can be achieved by contamination then removed by PDG. This is particularly evident in the plot for the 798 °C contamination in Figure 2. We have previously shown a linear correlation between iron loss and recombination activity of oxide precipitates.[5] This combined with the reversibility observation leads us to reinforce our previous conclusion that atomic (as opposed to precipitate-based) decoration of the oxide precipitates and

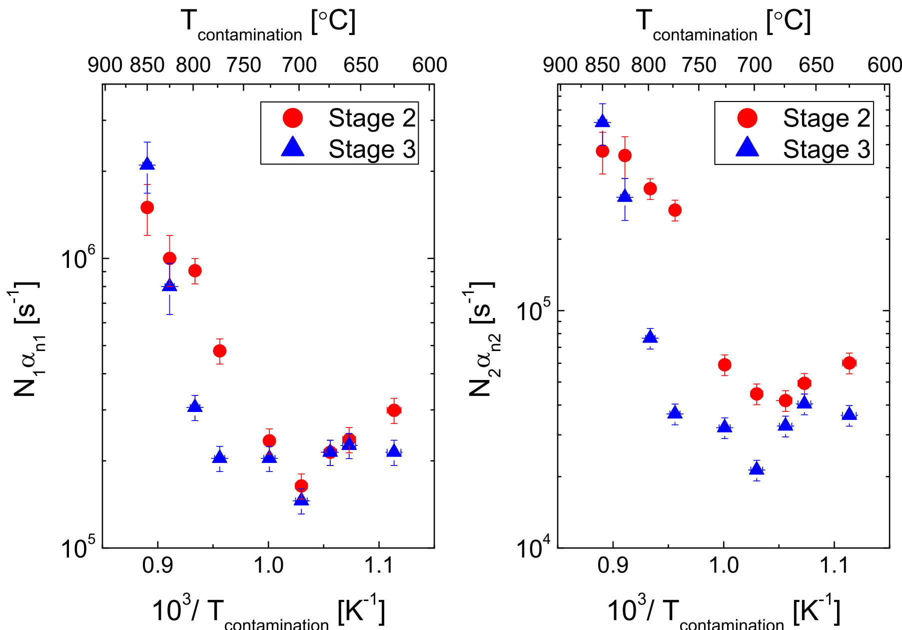

FIG. 5. Fitting parameters to the injection-dependent residual lifetime data for samples after iron contamination (Stage 2) and after PDG (Stage 3) as a function of iron contamination temperature.

associated defects occurs. The behaviour is different in samples contaminated at >850 °C. Such samples undergo a detrimental change in lifetime, which is not fully recoverable by the PDG process used. We suggest that the concentration of iron introduced by contamination at these higher temperatures (solubility $>1.2 \times 10^{13}\,\mathrm{cm}^{-3}$ (Refs. 19 and 20)) provides sufficient driving force for the nucleation of iron-containing precipitates during cooling after contamination. The cooling rate used here is very rapid, which limits the opportunity for nucleation of iron-containing precipitates in the bulk. It is therefore likely that iron precipitates in the vicinity of existing crystal defects, such as the oxide precipitates and surrounding dislocations/stacking faults. The co-precipitation of iron and oxygen in silicon has been found previously.[23,24] Precipitated iron is known to be difficult to getter,[25] and the PDG process used here confirms this.

There does appear to be a fundamental limit for the effect of the PDG process used. Figure 5 shows that the $N_i\alpha_{ni}$ parameters are at their minimum value after gettering for all samples contaminated at 726 °C and below. This could imply that iron interacts with oxide precipitates and associated defects in multiple ways, and only some of these interactions are overcome in our PDG process. We have previously postulated that iron preferentially interacts with precipitate corners[5,21] and further theoretical studies of the interaction of iron with such discontinuities would be beneficial.

Some samples in this study were subjected to a second PDG step. Whilst this was generally effective at further reducing the bulk iron concentration (Figure 4), in some cases it reduced the overall residual lifetime (Figure 2). The injection-dependence for samples subjected to a second PDG process is as expected for iron-contaminated oxide precipitates, so the oxide precipitates in some samples have become decorated with more impurities. The reason for this is not clear.

B. Competitive gettering

Oxide precipitates and associated defects are well known to act as gettering centres for metallic impurities, including iron.[26,27] PDG is also well known to getter iron.[6,7] Thus, in our samples, there are two gettering systems in place during thermal processing. How do these systems compete with each other?

The data presented in Figure 4 show that samples contaminated at 674 °C and above have reduced bulk iron concentrations after the first PDG process. Figure 5 shows that these samples experience no increase (and sometimes a significant decrease) in recombination activity. For example, samples contaminated at 798 °C experience a bulk iron concentration reduction of $1.8 \times 10^{12}\,\mathrm{cm}^{-3}$ during PDG, while the $\alpha_{n1}N_1$ and $\alpha_{n2}N_2$ parameters also reduce to 34% and 23% of their initial values, respectively. We have previously demonstrated a correlation between iron at oxide precipitates and associated defects and the resulting recombination activity.[5] The substantial concentration of bulk iron lost in many cases would give rise to a significant increase in recombination activity during gettering and this is not observed. Thus, we conclude that iron lost from the bulk does not segregate to the oxide precipitates and associated defects for these samples.

The question therefore remains, where does the iron known to be lost from the bulk go? Two options seem possible: (i) the iron forms precipitates in the bulk; or (ii) the iron is gettered to the phosphorus-diffused regions at the surfaces. The latter option seems likely for three main reasons:

(1) A second PDG process applied to some samples results in a further reduction of bulk iron concentration (Figure 4). This suggests that the gettering is kinetically limited by relatively long-range diffusion to surfaces.
(2) Iron precipitates are likely to exhibit different recombination properties to iron-decorated oxide precipitates, yet the injection-dependence of the residual lifetime has the same form before and after the PDG process (Figures 2 and 3).
(3) Insufficient driving force for precipitation. The bulk iron concentrations are generally lower than the equilibrium solubility at the gettering temperatures, so bulk iron is generally only supersaturated during cooling after gettering. The level of supersaturation at the relatively rapid cooling rate is unlikely to be sufficient for the formation of iron silicide precipitates.[20,28]

C. Implications for silicon photovoltaic solar cells

Oxide precipitates have been linked to a substantial reduction in conversion efficiency in monocrystalline silicon solar cells.[1] Recombination activity at oxide precipitates can arise via segregated impurity atoms[5] or via dangling bonds.[29,30] Dangling bond centres can be passivated with hydrogen,[31] and hydrogen passivation is likely to occur during cell processing. The recombination that occurs in a completed solar cell due to oxygen precipitation is therefore likely to arise from small concentrations of impurities segregated to the precipitates and surrounding defects. The results presented in this paper are generally positive with regards to relatively high quality monocrystalline silicon, as they show that iron can be gettered away from oxide precipitates by a PDG process. Optimisation of the time-temperature profile for the PDG process could provide larger improvements than those demonstrated here.

For silicon containing higher levels of contamination, the situation may well be different because the impurities form precipitates, which do not respond to PDG as well as atom-like decoration. This is supported by a recent study by Boulfrad *et al.*, who use oxide precipitates for internal gettering in mc-Si.[9] They find that PDG does not significantly improve lifetime after an internal gettering procedure. We suggest this is because the higher impurity level in mc-Si provides a higher degree of impurity supersaturation and this drives metal precipitation in the vicinity of oxide precipitates during cooling after their internal gettering process. In contrast, Rinio *et al.* have found external gettering to the emitter more likely than internal gettering,[32] but their gettering procedures were performed at lower temperatures, which would be insufficient to nucleate and grow oxide precipitates.

V. CONCLUSIONS

Oxide precipitates and associated defects (dislocations and stacking faults) are recombination active in silicon partly

because of iron segregated to them. In this study, we have systematically studied the contamination of oxide precipitate-containing silicon with iron, and how the material subsequently responds to PDG. For the conditions used, relatively low levels of bulk iron contamination ($<5 \times 10^{12}\,cm^{-3}$) result in an iron distribution at oxide precipitates and associated defects whose effect can be reversed by PDG. This suggests that the decoration is in the form of atomic iron at the oxide precipitates and associated defects. Higher levels of bulk iron contamination ($>1.2 \times 10^{13}\,cm^{-3}$) result in an iron distribution at oxide precipitates and associated defects which is not reversed by the PDG process used, and this implies iron precipitates in the vicinity of the defects. Bulk iron is generally preferentially gettered to the phosphorus diffused layer rather than the oxide precipitates and associated defects. Thus, silicon solar cells containing oxide precipitates and relatively low levels of iron contamination can have their performance improved by PDG.

ACKNOWLEDGMENTS

J.D.M. acknowledges financial support from a Royal Academy of Engineering/EPSRC Research Fellowship, an EPSRC First Grant (EP/J01768X/2), and a Royal Society Research Grant (RG100076). We are grateful to Radka Chakalova (University of Oxford) for assistance with sample cleaning and surface passivation, to staff at ISFH for assistance with PDG processing, and to Professor Peter Wilshaw (University of Oxford) for access to lifetime measurement facilities.

[1] J. Haunschild, I. E. Reis, J. Geilker, and S. Rein, Phys. Status Solidi RRL **5**, 199 (2011).
[2] R. Søndena, Y. Hu, M. Juel, M. S. Wiig, and H. Angelskår, J. Cryst. Growth **367**, 68 (2013).
[3] V. Kveder, M. Kittler, and W. Schröter, Phys. Rev. B **63**, 115208 (2001).
[4] M. Seibt, R. Khalil, V. Kveder, and W. Schröter, Appl. Phys. A **96**, 235 (2009).
[5] J. D. Murphy, K. Bothe, V. V. Voronkov, and R. J. Falster, Appl. Phys. Lett. **102**, 042105 (2013).
[6] S. P. Phang and D. Macdonald, J. Appl. Phys. **109**, 073521 (2011).
[7] V. Vähänissi, A. Haarahiltunen, H. Talvitie, M. Yli-Koski, and H. Savin, Prog. Photovoltaics: Res. Appl. **21**, 1127 (2013).
[8] P. Krenckel, P. Saring, M. A. Falkenberg, V. Kveder, and M. Seibt, Energy Procedia **38**, 582 (2013).
[9] Y. Boulfrad, A. Haarahiltunen, H. Savin, E. J. Øvrelid, and L. Arnberg, "Enhanced performance in the deteriorated area of multicrystalline silicon wafers by internal gettering," Prog. Photovoltaics: Res. Appl. (published online).
[10] O. Schultz, S. W. Glunz, S. Riepe, and G. P. Willeke, Prog. Photovoltaics: Res. Appl. **14**(8), 711 (2006).
[11] P. Karzel, M. Ackermann, L. Gröner, C. Reimann, M. Zschorsch, S. Meyer, F. Kiessling, S. Riepe, and G. Hahn, J. Appl. Phys. **114**, 244902 (2013).
[12] L. J. Geerligs, Y. Komatsu, I. Röver, K. Wambach, I. Yamaga, and T. Saitoh, J. Appl. Phys. **102**, 093702 (2007).
[13] H. J. Möller, C. Funke, A. Lawerenz, S. Riedel, and M. Werner, Sol. Energy Mater. Sol. Cells **72**, 403 (2002).
[14] J. D. Murphy, K. Bothe, R. Krain, V. V. Voronkov, and R. J. Falster, J. Appl. Phys. **111**, 113709 (2012).
[15] G. Zoth and W. Bergholz, J. Appl. Phys. **67**, 6764 (1990).
[16] D. H. Macdonald, L. J. Geerligs, and A. Azzizi, J. Appl. Phys. **95**, 1021 (2004).
[17] S. Rein and S. W. Glunz, J. Appl. Phys. **98**, 113711 (2005).
[18] J. D. Murphy, K. Bothe, M. Olmo, V. V. Voronkov, and R. J. Falster, J. Appl. Phys. **110**, 053713 (2011).
[19] J. D. Murphy and R. J. Falster, Phys. Status Solidi RRL **5**, 370 (2011).
[20] J. D. Murphy and R. J. Falster, J. Appl. Phys. **112**, 113506 (2012).
[21] J. D. Murphy, R. E. McGuire, K. Bothe, V. V. Voronkov, and R. J. Falster, Sol. Energy Mater. Sol. Cells **120**, 402 (2014).
[22] R. A. Sinton and A. Cuevas, Appl. Phys. Lett. **69**, 2510 (1996).
[23] W. Wijaranakula, J. Appl. Phys. **79**, 4450 (1996).
[24] M. Trushin, O. Vyvenko, W. Seifert, G. Jia, and M. Kittler, Phys. B **404**, 4645 (2009).
[25] D. P. Fenning, J. Hofstetter, M. I. Bertoni, S. Hudelson, M. Rinio, J. F. Lelièvre, B. Lai, C. del Cañizo, and T. Buonassisi, Appl. Phys. Lett. **98**, 162103 (2011).
[26] R. J. Falster and W. Bergholz, J. Electrochem. Soc. **137**, 1548 (1990).
[27] D. Gilles, E. R. Weber, and S. Hahn, Phys. Rev. Lett. **64**, 196 (1990).
[28] A. Y. Liu and D. Macdonald, J. Appl. Phys. **115**, 114901 (2014).
[29] V. Lang, J. D. Murphy, R. J. Falster, and J. J. L. Morton, J. Appl. Phys. **111**, 013710 (2012).
[30] M. Koizuka and H. Yamada-Kaneta, J. Appl. Phys. **88**, 1784 (2000).
[31] M. Koizuka and H. Yamada-Kaneta, J. Appl. Phys. **84**, 4255 (1998).
[32] M. Rinio, A. Yodyunyong, S. Keipert-Colberg, Y. P. B. Mouafi, D. Borchert, and A. Montesdeoca-Santana, Prog. Photovoltaics: Res. Appl. **19**, 165 (2011).